*Original Article*
# Barker-coded excitation in ophthalmological ultrasound imaging

Sheng Zhou, Xiao-Chun Wang, Jun Yang, Jian-Jun Ji, Yan-Qun Wang

*Institute of Biomedical Engineering Chinese Academy of Medical Sciences, Tianjin 300192, China*

**Abstract:** High-frequency ultrasound is an attractive means to obtain fine-resolution images of biological tissues for ophthalmologic imaging. To solve the tradeoff between axial resolution and detection depth, existing in the conventional single-pulse excitation, this study develops a new method which uses 13-bit Barker-coded excitation and a mismatched filter for high-frequency ophthalmologic imaging. A novel imaging platform has been designed after trying out various encoding methods. The simulation and experiment result show that the mismatched filter can achieve a much higher out signal main to side lobe which is 9.7 times of the matched one. The coded excitation method has significant advantages over the single-pulse excitation system in terms of a lower MI, a higher resolution, and a deeper detection depth, which improve the quality of ophthalmic tissue imaging. Therefore, this method has great values in scientific application and medical market.

**Keywords:** Barker, ultrasound, excitation imaging, decoded compression

## Introduction

In the clinical field, there are strict limits on the output intensity of diagnostic ultrasound equipment in order to prevent injuries on the human body from ultrasonic cavitation and thermal effects. Compared to other organs, the output parameters of ophthalmic ultrasonography are much stricter, such as spatial peak-temporal average intensity ($I_{SPTA.3}$), spatial peak-pulse average intensity ($I_{SPPA.3}$), and mechanical index (MI) [1]. Therefore, the ultrasonic intensity cannot be increased by simply increasing the amplitude of the single pulse.

Currently, the central frequency of the probe in ophthalmic A/B mode diagnostic ultrasound instruments is confined to 10 to 12 MHz, if there is the need for more detailed information on pathological tissues, the central frequency must be increased to 15 MHz, or even to 20 MHz, to improve the resolution of superficial tissue imaging, such as lens, vitreous, and retinal tissues. Although high frequencies can improve resolution, the exponential increase in attenuation with frequency makes detection of faintly reflective fluid vitreous interfaces problematic as frequency is increased [2]. Furthermore, the

deep echo information from orbital tissues will be lost and thus the panoramic imaging will not be achieved. This greatly influences the value of ultrasound application in ophthalmic clinical diagnosis.

With coded excitation method, the problem mentioned above can be solved. It will not only meet the requirements of output parameters, but also improve the signal-to-noise ratio (SNR), resolution, and thus image quality. This technology, called Digital Encode Ultrasound (DEU), draws inspiration from spread spectrum technology in radar communication [3, 4] which uses pulse-compression from communication theories. The conventional single-pulse excitation is replaced by long coded pulse excitation, which can extend the pulse duration instead of increasing the single pulse amplitude. In this way, the average transmitting energy can be increased dramatically. At the meantime, by compressing the code energy into a very short time interval, the system SNR, and penetrability [5] are increased as well.

The coded excitation technique was first introduced to medical ultrasonic imaging by Newhouse in 1974. At the same time, he pro-

**Table 1.** Different types of codes

|  | Single-Tx | Multiple-Tx |
|---|---|---|
| Phase Coding | Barker, M-sequence | Golay |
| Frequency Coding | Chirp | |

posed an ultrasonic imaging system with coded white noises and a Doppler testing system [6-8]. In the following 30 years, coded excitation technique has been fully developed. Nowadays, many research institutions, such as The Fast Imaging Laboratory in The Technical University of Denmark, The Ultrasonic Department in The Polish Academy of Sciences [9], The Riverside Research Institute [10-13], UIUC [14, 15] and Tsinghua University, are still conducting research on these aspects and obtaining new results [16-18]. For ophthalmologic imaging, some researchers fabricated an annular array ultrasound transducer with a 17 to 20 MHz center frequency, implemented a synthetic-focusing algorithm to extend the depth-of-field, and used a pulse-encoding strategy to increase sensitivity.

The excitation codes are categorized according to whether they use a single transmit or multiple transmit and whether they use phase coding or frequency coding, as shown in **Table 1** [5].

Chirp code is a possible ideal choice for ultrasonic imaging systems because the pulse-compression is minimally affected by nonlinear factors such as attenuation and beam forming. Also, it is a single transmitting code which is minimally affected by tissue movement. However, its transmitting voltage of multiple amplitudes has higher requirement for the hardware. In most digital high-frequency ultrasonic equipment, binary phase codes are adopted as the transmitting codes considering the system complexity. Using the Golay complementary codes for imaging is to have two transmits for each focal-zone. The decoding process is as follows: After the first firing with code A, the return echo is correlated with the corresponding decode filter A and saved in a memory buffer. Subsequently code B is fired, echo is filtered with decode filter B, and the two filtered waveforms are summed to complete the decoding process [5]. The Golay complementary sequence can completely eliminate the side-lobes. However, the mechanism of double transmitting is easily influenced by moving tis-

sues and thus will lead to errors. Although eyes are basically stationary tissues, the mechanical sector-scanning probe will have some effect on imaging. For M-sequence and Barker codes, the pulse-compression effect of the M-sequence is not as good as the Barker code. Furthermore, the concept of an optimum coded sequence, and the calculating method proved that Barker codes were optimum sequences except when the code number N is 11 [17, 19, 20]. Another study experimentally verified the application of 13-bit Barker codes for high-frequency ultrasound imaging [21].

A theory and practical performance of Barker codes for CFI have been studied in one paper [22] and the resultant color flow images demonstrate the expected improvements in penetration and axial resolution. A 13-bit Barker code was adopted in paper [23] and the pulse-compression was achieved by using a pseudo-inverse filter in the frequency domain. The sidelobe level was below -60 dB and the acoustic output intensity satisfied the limits set by The Food and Drug Administration [1]. In another paper [24], a 13-chip Barker-coded excitation pulses was applied to improve the sensitivity of emboli detection in transcranial Doppler (TCD) ultrasound systems. The simulation results indicated that the TCD system using coded excitation was more sensitive for faster and smaller emboli, which was significant for early diagnosis of stroke.

However, the majority of research was limited to theory simulations and the entire medical ultrasound imaging system was rarely implemented. Based on the analysis above, we choose the 13-bit Barker code as the excitation code for our digital ultrasonic diagnostic system.

Currently, two common pulse-compression methods are matched filter and mismatched filter method. For Golay and Chirp codes, the matched filter method results in a low sidelobe levels with relatively straightforward design and implementation methods. For Barker codes, although the matched filter method can achieve the lowest sidelobe levels, the mainlobe levels are N times of the sidelobe, where N is the number of Barker bits. For Barker codes, the largest number is of 13 bits. Therefore, the SNR is 11.1 dB with the matched filter method and the peak sidelobe level (PSL) is -22 dB [5].
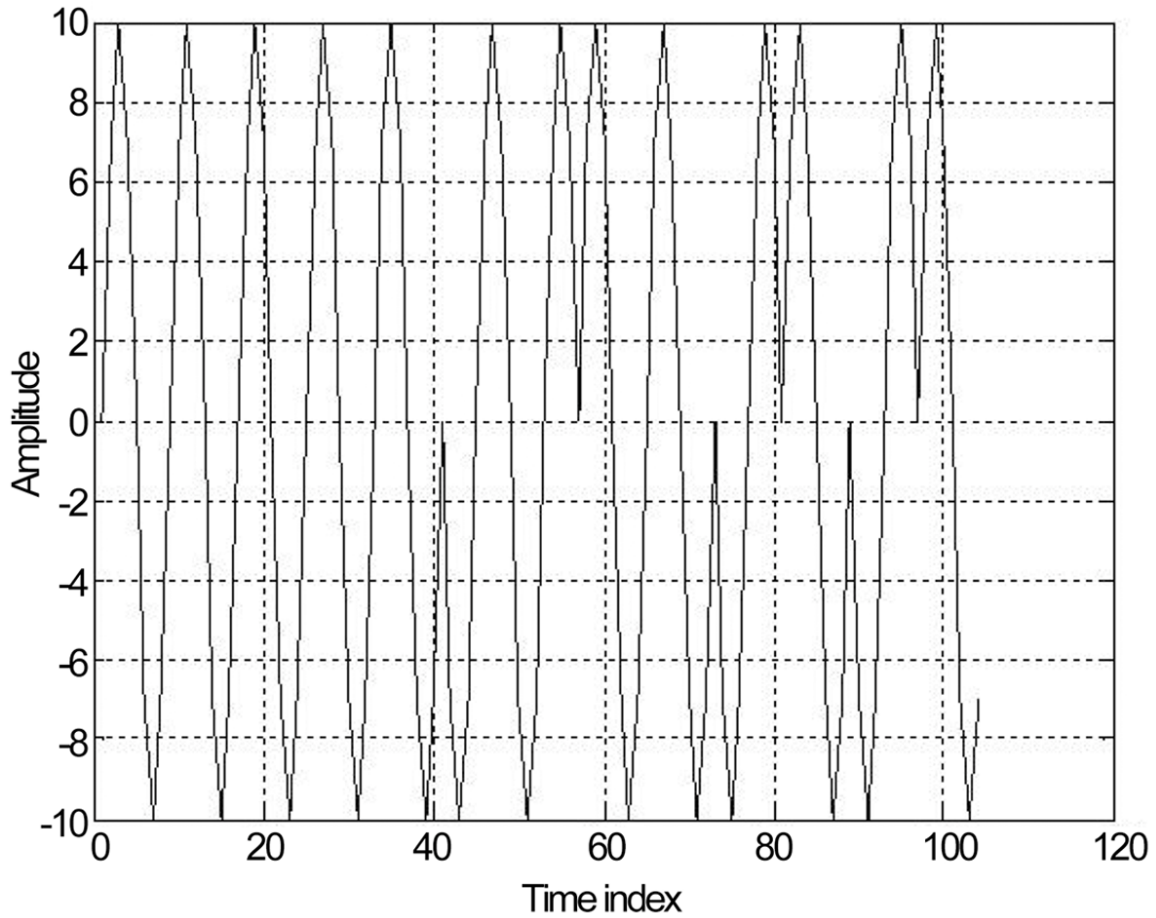
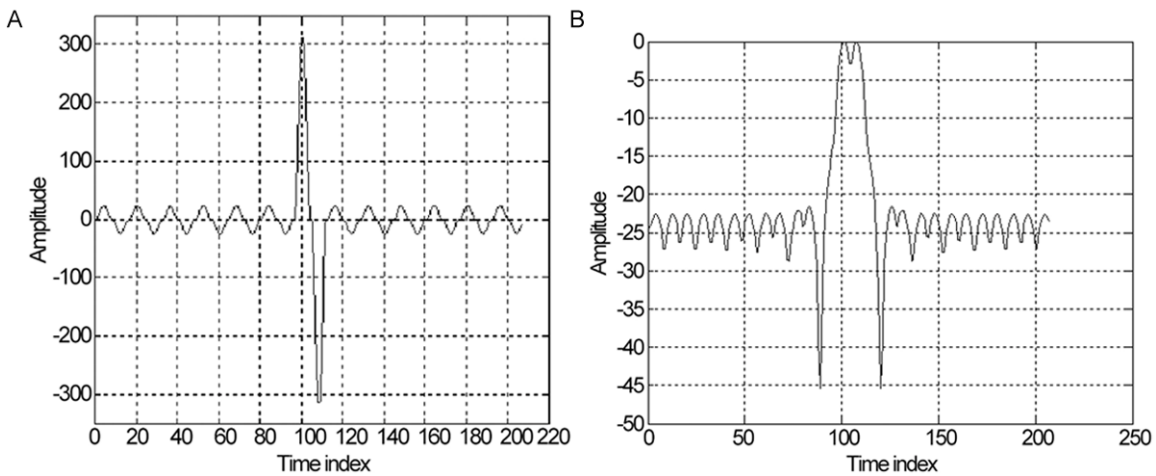**Figure 1.** Simulated waveforms of the 13-bit Barker codes.



**Figure 2.** Simulated results by the matched filter. A. The convolution results; B. The envelope of the results.

These results indicate that the range sidelobe is not inhibited by the matched filter [18]. Therefore, some mismatched filters [21, 25] such as the inverse filter [26, 27], Wiener filter [28], and spike filter [29] are designed for pulse-compression. They can obtain better range sidelobe compression, although with a slight loss of SNR.
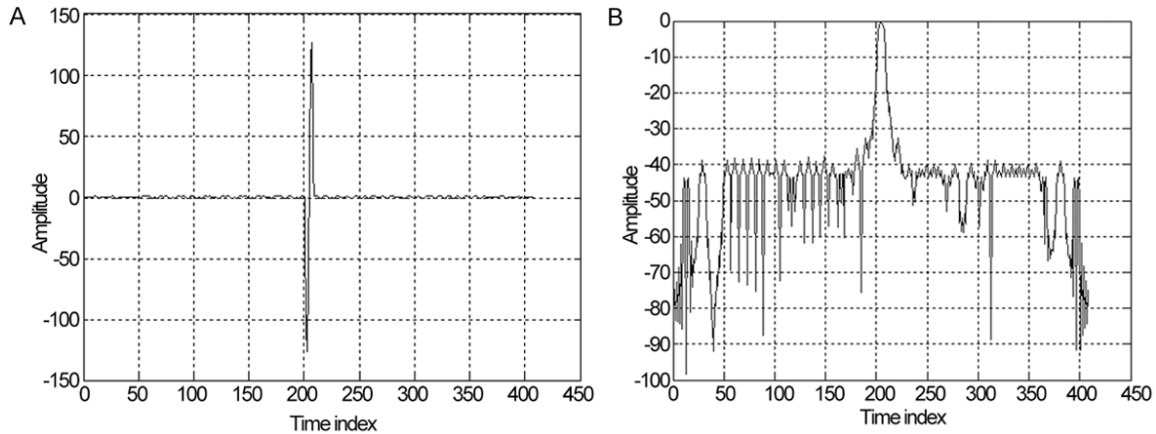
**Figure 3.** Simulated results of the mismatched filter. A. The convolution results; B. The envelope of the results.

On the basis of previous achievements, an ultrasonic transmitting and receiving platform with coded excitation and pulse-compression is developed and stated in this report. The ophthalmic ultrasound images were processed and displayed on a computer with transferring by a USB interface.

To compare the advantages and disadvantages of each pulse-compression method, in this study, we performed simulated experiments using the matched filter and mismatched filter methods.

**Materials and methods**

*Simulation*

Binary 13-bit Barker codes are composed of [+1, +1, +1, +1, +1, -1, -1, +1, +1, -1, +1, -1, +1]. Since the sampling frequency is 8 times of the echo frequency, we choose the following sequence composed of 8 sampling points for each cycle. The -1 is expressed as [0, -7, -10, -7, 0, 7, 10, 7] and the +1 is expressed as [0, 7, 10, 7, 0, -7, -10, -7]. **Figures 1**, **2** show the MATLAB-simulated waveforms of Barker codes; **Figure 1** shows the 13-bit Barker waveform and **Figure 2** shows the result after the matched filter. In **Figure 2A**, the peak-peak level of the main lob is ±312, the peak-peak level of the sidelobe is ±24, and the mainlobe/sidelobe ratio is 13. **Figure 2B** shows the envelope of the matched filter result, where the sidelobe attenuation is -22.3 dB.

**Figure 3A** shows the result of the 13-bit Barker codes with the mismatched filter. The order

number of the mismatched filter designed in this experiment is: *P* = 3, N = 39. That is, the mismatched filters are three times longer than the signal length. The PSL optimized filter was obtained using MATLAB's constrained optimization function fmincon. The peak to peak level of the main lobe is ± 127, with sidelobe ± 1. Therefore, the main-side ratio is 127, which is 9.7 times of the matched filter. This means that although the mismatched filter decrease the level of the main lobe, with the sidelobe level effectively decreased, the contrast is dramatically improved and the clutter artifacts are reduced. **Figure 3B** shows the envelope of the mismatched filter result, in which the sidelobe attenuation is -42 dB.

*Design of the system*

The coded excitation systems and traditional single-pulse imaging systems differ in the following aspects: 1. Using coded excitation in the transmitting circuit and thus the length is longer than the single-pulse excitation; and 2. The receiving circuit needs to compress the pulses of the echo signals, and thus the calculation amount is larger. Therefore, there are some special requirements for the coded excitation experimental system: 1. The transmitting circuit must be able to generate different coded excitations; and 2. Different from the motion organs as the heart, eyes are the basically stable organs, so we chose the 10 fps as the system imaging frame rate which is already meet the requirements in clinical; 3. Each frame is constructed with 512 lines and each line is included of 768 points. In conclusion, the FPGA needs to have the function of imaging this num-
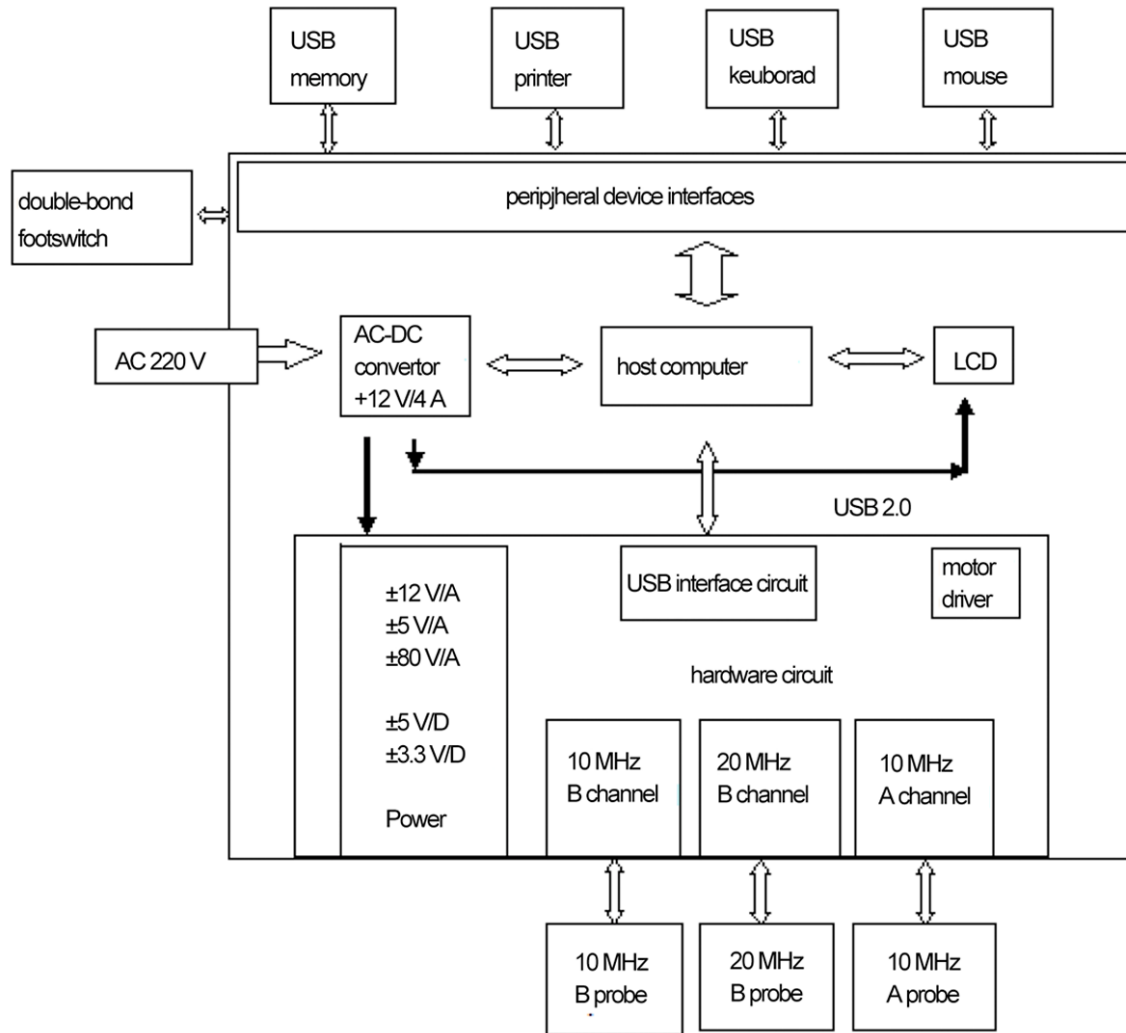
**Figure 4.** Block diagram of the system.

ber of excitation echoes and real-time pulse-compression.

**Figure 4** shows the block diagram of the whole system, which includes a host computer, hardware circuit, three ultrasonic probes, an LCD display, footswitch, and USB peripheral device and etc. The embedded industrial control main board is chosen as the host computer for miniaturization and portability of the whole system. The functions of the host computer are to receive the underlayer data and process and control the software in real time. A single-element mechanical scanning probe is used in this experimental system, with three probes: a 10 MHz B-mode probe, a 20 MHz B-mode probe, and a 10 MHz A-mode probe, which are separately applied for ophthalmic panoramic imaging, ophthalmic tissue high-frequency imaging,

and ophthalmic tissue bio-measurements. A LCD display is used for the real-time image displaying. A double-foot switch is used to start and freeze the probe. USB peripheral devices such as memory, printer, mouse, and key panel improve the operability of the overall system.

Hardware circuit is the core component of the entire system. A FPGA (field-programmable gate array) and its peripheral circuit is the core of the entire hardware circuit. An EP3C55 FPGA of the Cyclone III series designed by ALTERA Corporation is adopted and it controls the mechanical sector-probe deflection, image display synchronization, and the USB interface logics.

The pulse level of the four coded pulse sequences generated by the FPGA is increased from 3.3

V to 12 V by the MOSFET trigger circuit in order to excite the transmitting circuit. The transmitting circuit is constructed using two bipolar pulse-transmitting chips, which results in a return-to-zero function. The transmitting voltage is ± 80 V. After the transmitting circuit, the coded sequences are changed to bipolar pulse sequences in order to excite the ultrasonic transducer. After a high-voltage isolation circuit, the echo signals enter the pre-amplifier and variable-gain control circuit. The gain of the pre-amplifier is ranged from 10 to 15 dB. The FPGA generates the time gain control (TGC) line data to control the variable-gain amplifier in order to make the gain variables 50 dB. The main clock in this experiment system is 80 MHz. High-speed A/D chips work at 80 MHz and 120 MHz in different modes. Its sampling precision is 14 bits and its sampling mode is set by the FPGA via an SPI interface.

The digital signal processing of the ultrasonic echoes by the FPGA is as follows: high-frequency data sampling and loading to the memory; digital filtering; digital demodulation; logarithm transformation; secondary sampling; and uploading to the computer. The echo data after digital signal processing are loaded into the SRAM and then uploaded to the computer via a USB 2.0 interface circuit. Finally, the system can be operated and controlled through a human-machine interface.

*Realization of matched filter and mismatched filter based on FPGA*

The realization of FPGA for matched filtering of 13-bit Barker codes is relatively easy. For the sequences are composed of 8 sampling points for each cycle, and the Barker codes is 13 bits, it is needed to open up a 14-bit memory space with a depth of 13 × 8 for convolution decoding. The echo data are unchanged for decoding filter coefficient + 1, and are taken as the opposite of the complementary codes for -1. Then, the matched filter results are achieved by adding them in parallel.

The design schematic of FPGA for the mismatched filter is as follows. Firstly, the mismatched-filter coefficients are quantified by multiplying by $2^7 = 128$ and loaded into the RAM in the FPGA after rounding. Secondly, the real-time echo matrix is constructed. Thirdly, each row in the matrix is multiplied by the cor-

responding coefficient. Fourthly, the multiplied result is added one by one for 39 rows. Fifthly, the added results are divided by the quantified number to obtain the results of the mismatched-filter decoding compression.

*Experiments*

We performed four sets of experiment to evaluate the effectiveness of Barker-coded imaging versus conventional single-pulse imaging.

A single reflector echo experiment was designed to compare the compression effects between using a matched filter and a mismatched filter in the practical application. Coded excitation was generated by an FPGA and then transmitted through a circuit to excite the 10 MHz ultrasonic transducer. The transducer transmitted ultrasonic waves and the waves were reflected by a single surface and generated echo signals. After amplification and sampling with an A/D converter, the echo signals were input into the FPGA for data processing and decoding pulse-compression. Finally, the data were displayed on an oscilloscope through a D/A converter.

Our second experiment investigated whether coded excitation increases SNR and penetration depth relative to what can be achieved with conventional single-pulse imaging. For this experiment, a tissue-mimicking phantom (KS107BG, Institute of Acoustics, Chinese Academy of Sciences) was scanned using Barker-coded excitation and single-pulse excitation. The phantom has an attenuation of 0.7 dB/cm/MHz near 10 MHz.

The third was a resolution measurement experiment. The probe we used in this system is a one array element probe. The lateral resolution of the probe is determined by the adopted transducer. The coded excitation and decoded compression have no influence to its lateral resolution. So we only need to test the axial resolution after coded excitation. The testing module is seen as **Figure 5**. There are two tungsten wires with the diameter of 10 um between two screw fixed points. The distance between two tungsten wires are 0.2 mm and 0.3 mm. The testing wire target is put to a water channel which is spread with sound absorption materials in the bottom. The arrangement orientation of the wires is as the same as the ultrasound waves transmission orientation, that is, the
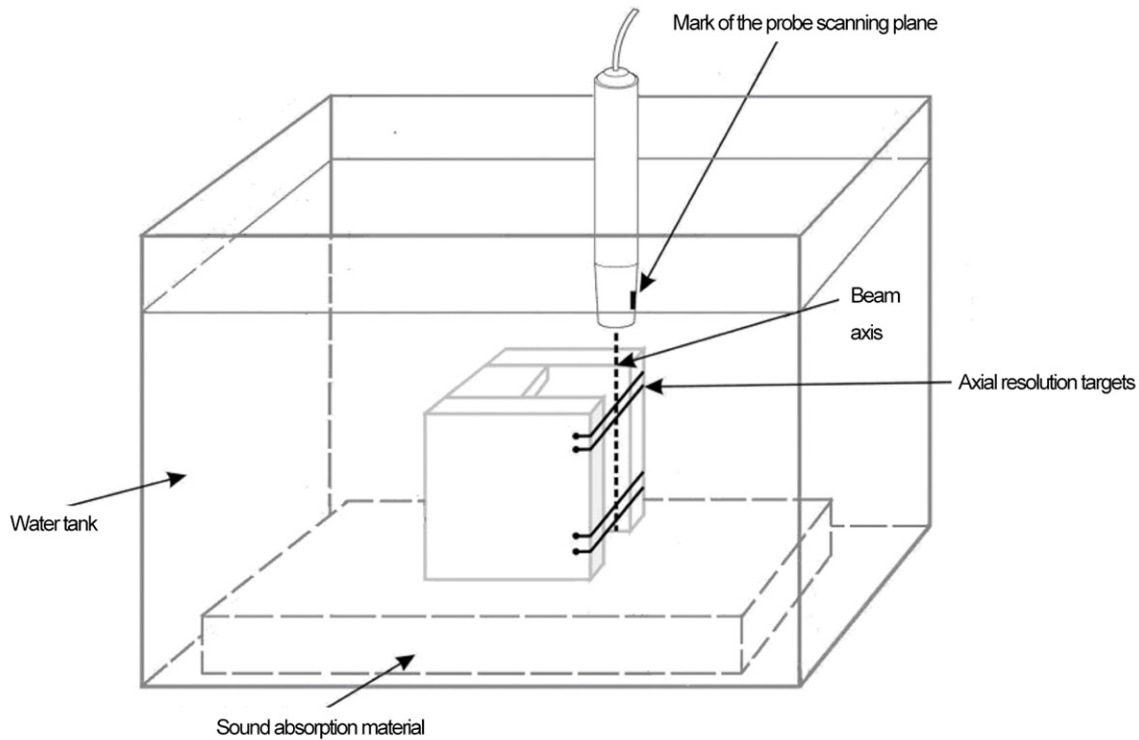
**Figure 5.** The measurement of axial resolution.

arrangement plane of the parallel wires is vertical with the probe surface. The probe is put above the testing target, and is scanned on the plane vertical with the target wires. The gain, brightness and contrast are adjusted to the optimum position. The distance between probe and target wire is adjusted to 23~24 mm. Micromotion of the probe angle and then the minimum distance separated by the tungsten wires on the images is the minimum axial can be achieved.

Finally, we evaluated the Barker coded imaging method in vivo. Images of a normal human eye were formed for each imaging method. The images were then qualitatively assessed.

### Results

*Single reflector echo experiment*

**Figure 6A** shows the 13-bit Barker coded excitation waves when the transmitting voltage was ±80 V. **Figure 6B** shows the echo signals from a single reflector surface. **Figure 7** shows the 13-bit Barker coded echo signals after the matched filter and mismatched filter, respectively. For these data, the A/D converter was 14 bits and the D/A converter was only 10 bits,

and the signals after the matched and mismatched filters was 18 bits and 22 bits, respectively. **Figure 7** shows the real-time echoes displayed on the oscilloscope. From **Figure 7A**, it can be seen that the peak value of the echo from the reflector surface after the matched filter decoding is 0.6 V, in which the highest sidelobe peak value is 0.15 V. In ultrasonic echoes, strong sidelobes overshadow weak signals and influence the imaging quality. Therefore, there is practical significance to inhibit the pulse-compression sidelobe levels. From **Figure 7B**, we can see that the 13-bit Barker coded excitation echoes has an effective sidelobe inhibition after the mismatched filter decoding, where the peak value is 0.72 V, with the highest sidelobe peak value 0.06 V. That means the mismatched filter increases the main-side ratio and decreases the sidelobe levels. Therefore, the mismatched filter is chosen for pulse-compression in our B-mode imaging system.

*Ultrasound phantom experiment*

**Figure 8** shows the phantom images. The dynamic range of these images is set to 60 dB to help demonstrate how the methods perform in terms of SNR. From the two images, we can
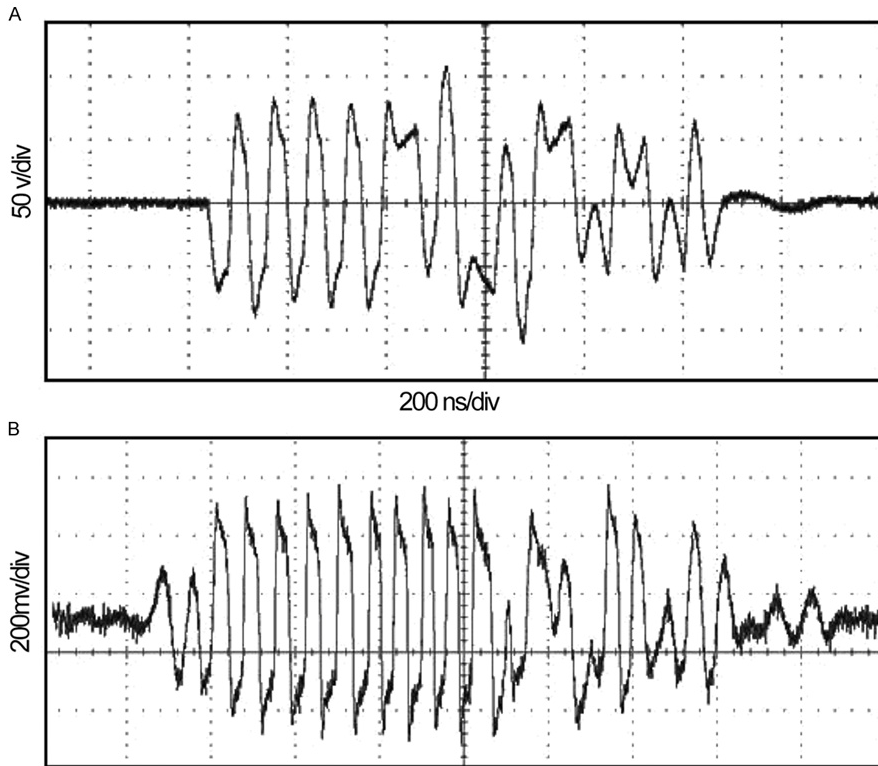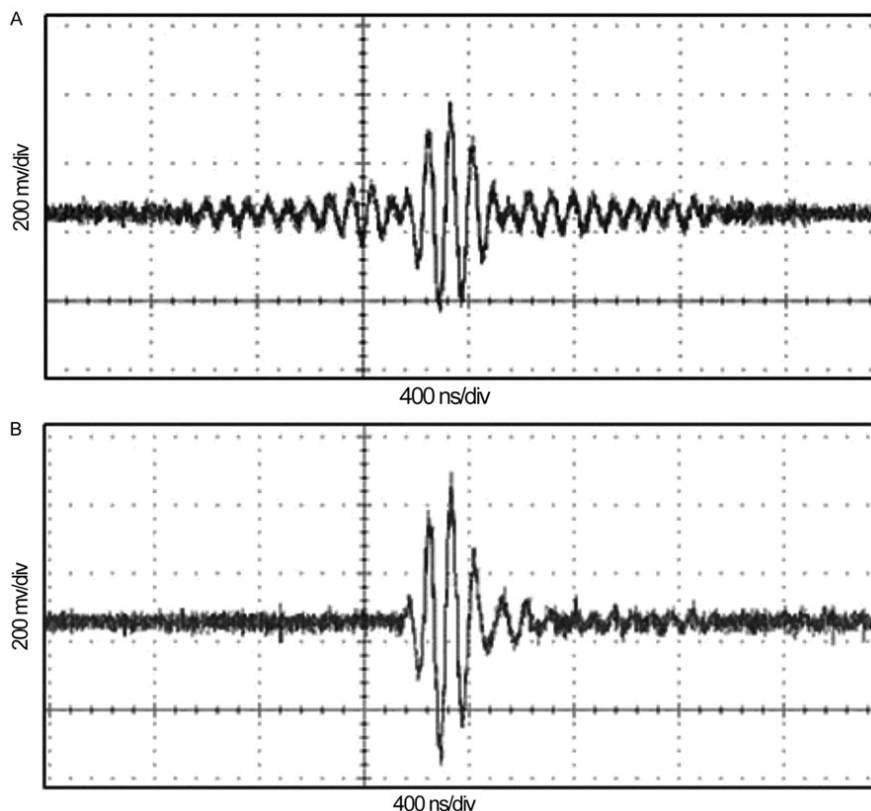
A

50 v/div

200 ns/div

B

200mv/div

**Figure 6.** Waveforms displayed on an oscilloscope. A. 13-bit barker coded excitation waveforms. B. Echo signals from one reflection surface excited by 13-bit Barker coded excitation.

A

200 mv/div

400 ns/div

B

200 mv/div

400 ns/div

see the Barker-coded excitation contribute to increasing the effective penetration depth. Compared to the 40 mm depth in **Figure 8A** by single-pulse excitation, the maximum effective penetration depth in **Figure 8B** by Barker-coded excitation is 50 mm and the much weaker signals can be obtained.

*Resolution measurement experiment*

**Figure 9** is the axial resolution testing result on the A mode using 10 MHz. From the figure we see that when the distance between tungsten wires is 0.2 mm, the two echo surfaces could be received clearly. So, the axial resolution of the system is not more than 0.2 mm. This result is as the same as the single-pulse excitation system and it is proved that the digital coded excitation and decoded compression technique can maintain the same axial resolution as the traditional single pulse excitation system.

*Imaging of the ophthalmic tissues*

**Figure 10** shows the ophthalmic B-

**Figure 7.** Decoded echo signals from single reflector surface. A. Using the matched filter. B. Using the mismatched filter.
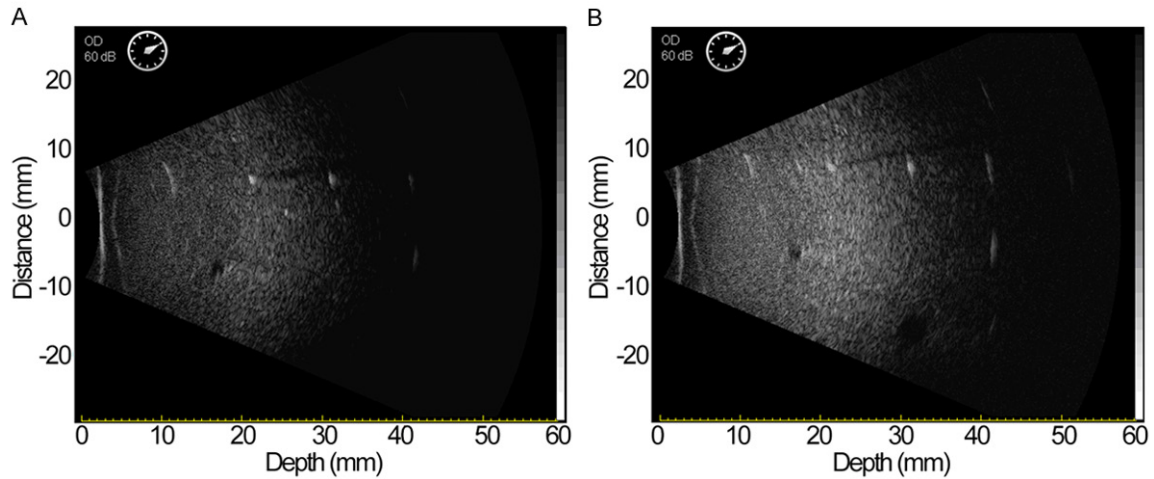


**Figure 8.** Images of tissue-mimicking phantom using a 10 MHz probe. A. Single-pulse excitation. B. 13-bit Barker coded excitation.
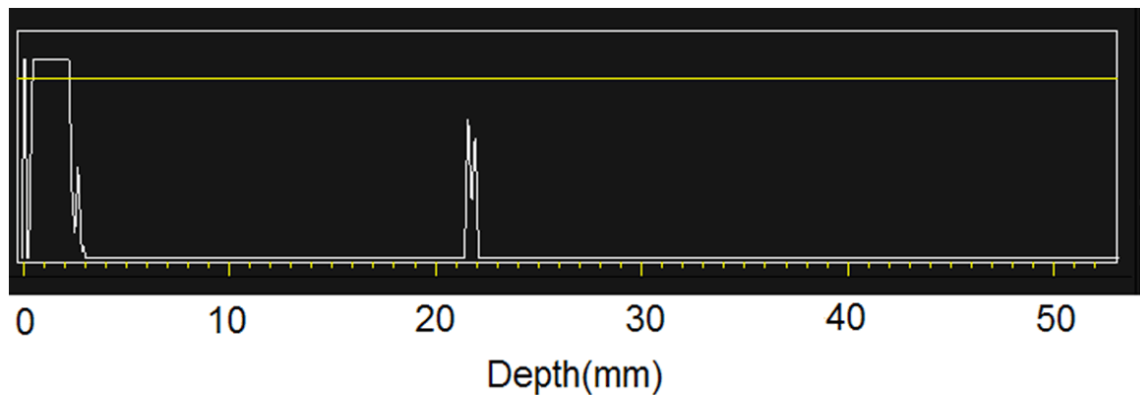


**Figure 9.** Axial resolution testing result, D = 0.2 mm.

mode images using a 10 MHz probe when the dynamic range is 60 dB. **Figure 11** shows the images using a 20 MHz probe when the dynamic range is 87 dB.

**Figures 10**, **11**. (A) shows the conventional single-pulse image and (B) shows the 13-bit Barker coded excitation with decoded using the mismatched filter.

Upon comparing the two-dimensional ophthalmic images, as well as the resolution measurement of the thread target, it can be seen that on the premise of keeping the axial resolution to 0.2 mm of 10 MHz probe and 0.1 mm of 20

MHz probe, and also the constant ground noise, the coded excitation and pulse-compression effectively increase the signal penetration depth and improve the image SNR. Moreover, the Barker coded excitation allows for the display of weaker reflectors. It could be diagnostically significant.

**Discussion**

A digital ophthalmic high-frequency ultrasonic imaging platform was proposed in this paper. Barker codes were chosen as the coded excitation in the system, which used a USB interface to send the image data to a host computer for
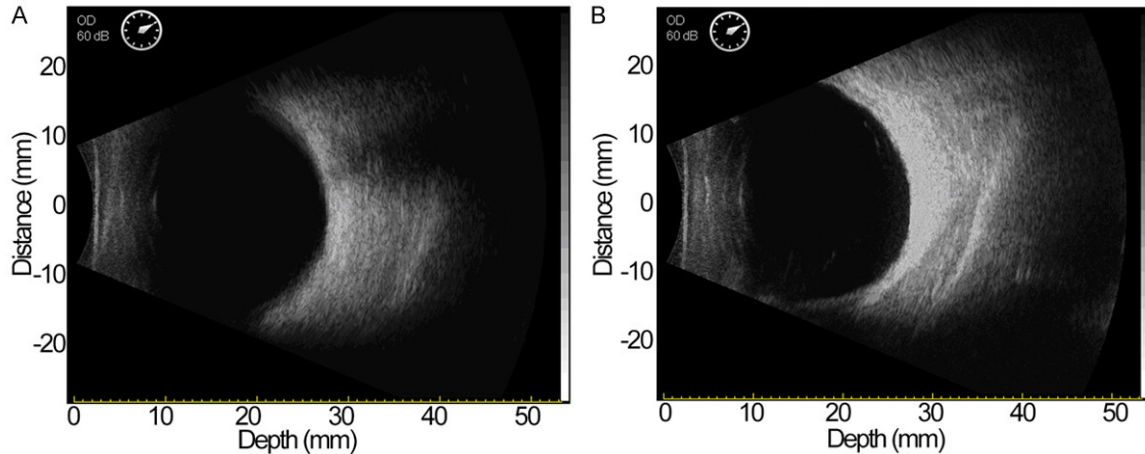
**Figure 10.** Ophthalmic B-mode images with a 10 MHz probe. A. Single-pulse excitation. B. 13-bit Barker coded excitation.
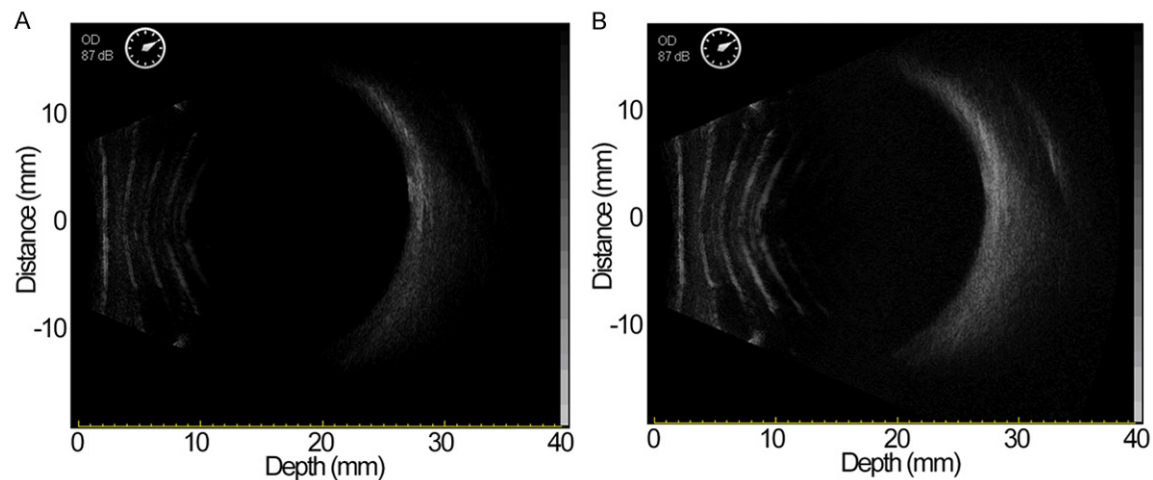


**Figure 11.** Ophthalmic B-mode images with a 20 MHz probe. A. Single-pulse excitation. B. 13-bit Barker coded excitation.

processing and display. The results indicated that the SNR of coded excitation echoes was superior to that of a single-pulse excitation. The resolution of the coded excitation image was the same without obvious sidelobe. However, the imaging depth and noise level were better than the single-pulse excitation. Furthermore, the coded excitation system significantly improved the weaker signals. Because of this, this system can be used to detect maladies such as vitreous opacity, and thus has practical applicability to ophthalmic diagnosis.

The coded excitation technique was realized in this design, but left scope for several topics to be further discussed and researched in depth. These included the following: for ultrasonic transducers with different bandwidths, we should add windows for the codes of excitation signals corresponding to the transducer's frequency bandwidth to make full use of the ultrasonic transducer's transferring capability; we should use the basis sequence modulation technique to improve the quality of long-coded excitation signals; in the procedure of pulse-compression simulation, we should use sidelobe inhibition methods such as linear programming theory, least squares technique, and iterative algorithm to attain a better pulse-compression effectiveness and minimize the sidelobe in a strong reflector interface; in order to further reduce $I_{SPPA.3}$ and MI, we should decrease the transmitting voltage and observe its influence on imaging quality, and select appropriate encoding and decoding methods.

## Disclosure of conflict of interest

None.

Address correspondence to: Yan-Qun Wang, Institute of Biomedical Engineering Chinese Academy of Medical Sciences, No.236 Baidi Road, Tianjin 300192, China. E-mail: wangyanqundd@163.com

## References

[1] Administration USFaD. Information for Manufacturers Seeking Marketing Clearance of Diagnostic Ultrasound Systems and Transducers. 2008.

[2] Hewick SA, Fairhead AC, Culy JC and Atta HR. A comparison of 10 MHz and 20 MHz ultrasound probes in imaging the eye and orbit. Br J Ophthalmol 2004; 88: 551-555.

[3] Simon MK, Omura JK, Scholtz RA and Levitt BK. New York: McGraw-Hill Inc; 1994.

[4] Brookner E. Phased array radars. Scientific Amer 1985; 52: 94-98.

[5] Chiao RY and Hao X. Coded excitation for diagnostic ultrasound: a system developer's perspective. IEEE Trans Ultrason Ferroelectr Freq Control 2005; 52: 160-170.

[6] Liu K and Gao SK. Study of optimal binary sequences in ultrasound imaging system using coded excitation. Chin J Biomed Engineer 2007; 26: 42-47.

[7] Newhouse VL. Pseudo-random characterization of time-varying media. New York: Springer-Verlag; 1988. pp. 281-290.

[8] Newhouse VL. Pseudo-random multimode operation. New York: Springer-Verlag; 1988. pp. 291-301.

[9] Nowicki A, Trots I, Lewin PA, Secomski W and Tymkiewicz R. Influence of the ultrasound transducer bandwidth on selection of the complementary Golay bit code length. Ultrasonics 2007; 47: 64-73.

[10] Mamou J, Ketterling JA and Silverman RH. Chirp-coded excitation imaging with a high-frequency ultrasound annular array. IEEE Trans Ultrason Ferroelectr Freq Control 2008; 55: 508-513.

[11] Mamou J, Ketterling JA and Silverman RH. High-frequency Pulse-compression Ultrasound Imaging with an Annular Array. Acoustical Imaging. Springer; 2009. pp. 81-86.

[12] Mamou J, Aristizabal O, Silverman RH, Ketterling JA and Turnbull DH. High-frequency chirp ultrasound imaging with an annular array for ophthalmologic and small-animal imaging. Ultrasound Med Biol 2009; 35: 1198-1208.

[13] Silverman RH, Ketterling JA, Mamou J, Lloyd HO, Filoux E and Coleman DJ. Pulse-encoded ultrasound imaging of the vitreous with an annular array. Ophthalmic Surg Lasers Imaging 2012; 43: 82-86.

[14] Sanchez JR and Oelze M. An ultrasonic imaging speckle-suppression and contrast-enhancement technique by means of frequency compounding and coded excitation. IEEE Trans Ultrason Ferroelectr Freq Control 2009; 56: 1327-1339.

[15] Sanchez JR, Pocci D and Oelze ML. A novel coded excitation scheme to improve spatial and contrast resolution of quantitative ultrasound imaging. IEEE Trans Ultrason Ferroelectr Freq Control 2009; 56: 2111-2123.

[16] Peng Q and Gao S. [Coded excitation and its applications in medical ultrasound imaging]. Sheng Wu Yi Xue Gong Cheng Xue Za Zhi 2005; 22: 175-180.

[17] Ruprecht J and Rupf M. On the search for good aperiodic binary invertible sequences. IEEE Trans Infor Theor 1996; 42: 1604-1612.

[18] Deng X and Fan P. New binary sequences with good aperiodic autocorrelations obtained by evolutionary algorithm. IEEE communications letters 1999; 3: 288-290.

[19] Liu K. Research on coded excitation in medical ultrasound imaging. Beijing: Tsinghua University; 2006.

[20] Zhao Y. Research on Coded Excitation in Ultrasound Color Flow Imaging System. Beijing: Tsinghua university; 2006.

[21] Misaridis T and Jensen JA. Use of modulated excitation signals in medical ultrasound. Part I: Basic concepts and expected benefits. IEEE Trans Ultrason Ferroelectr Freq Control 2005; 52: 177-191.

[22] Zhao H, Mo LY and Gao S. Barker-coded ultrasound color flow imaging: theoretical and practical design considerations. IEEE Trans Ultrason Ferroelectr Freq Control 2007; 54: 319-331.

[23] Udesen J, Gran F, Hansen KL, Jensen JA, Thomsen C and Nielsen MB. High frame-rate blood vector velocity imaging using plane waves: simulations and preliminary experiments. IEEE Trans Ultrason Ferroelectr Freq Control 2008; 55: 1729-1743.

[24] Lei X, Heng Z and Shangkai G. Barker code in TCD ultrasound systems to improve the sensitivity of emboli detection. Ultrasound Med Biol 2009; 35: 94-101.

[25] Haider B, Lewin PA and Thomenius KE. Pulse elongation and deconvolution filtering for medical ultrasonic imaging. IEEE Trans Ultrason Ferroelectr Freq Control 1998; 45: 98-113.

[26] Wilhjelm JE and Pedersen PC. Target velocity estimation with FM and PW echo ranging Doppler systems I. Signal analysis. IEEE Trans Ultrason Ferroelectr Freq Control 1993; 40: 366-372.

[27]  Oppenheim VS. Geophysical Signal Analysis. Englewood Cliffs, NJ: Prentice-Hall; 1980.

[28]  Robinson EA and Treitel S. Geophysical Signal Analysis. Englewood Cliffs, NJ: Prentice-Hall; 1980.

[29]  Hu CH, Liu R, Zhou Q, Yen J and Kirk Shung K. Coded excitation using biphase-coded pulse with mismatched filters for high-frequency ultrasound imaging. Ultrasonics 2006; 44: 330-336.